Sustainable Energy, Grids and Networks 35 (2023) 101141

Contents lists available at ScienceDirect

Sustainable Energy, Grids and Networks

journal homepage: www.elsevier.com/locate/segan

Design of cost functions for the real-time control of microgrids hosting distributed energy-storage systems

Plouton Grammatikos [a,*], Mario Paolone [a], Jean-Yves Le Boudec [b]

[a] Distributed Electrical Systems Laboratory, École Polytechnique Fédérale de Lausanne, Switzerland
[b] Laboratory for Communications and Applications, École Polytechnique Fédérale de Lausanne, Switzerland

ARTICLE INFO

Article history:
Received 23 September 2022
Received in revised form 31 March 2023
Accepted 6 August 2023
Available online 9 August 2023

Keywords:
Real-time control
Optimization-based control
Objective balancing
Energy storage systems
Microgrids

ABSTRACT

The research of this paper is framed in the context of multi-layered, optimization-based approaches for microgrid control. Specifically, we focus on the design of real-time objectives that are typically proxies of long-term ones. Examples include tracking a predetermined dispatch plan or a battery state-of-charge trajectory while satisfying the grid's operational constraints. If there is no formalized way of choosing the cost functions that reflect these objectives, an arbitrary choice could lead to a biased control in favor of certain objectives. The common approaches of configuring microgrid controllers usually rely on "oracle-based" approaches assumed to know exactly the studied scenarios. In this paper, we formalize the design goals of a real-time microgrid-control system by employing distributed energy-storage systems, and we give guidelines on how to design cost functions that satisfy them. Our method requires only certain parameters that can be chosen intuitively and gives a priori insight on the controller's behavior. The application of the theoretical work is verified in multiple scenarios by simulations performed using a realistic model of a microgrid.

1. Introduction

The transition from conventional bulk power generation to distributed generation has created new opportunities for grid operators to participate in the electricity market in an active way [1]. Active Distribution Networks (ADNs) and microgrids are becoming more widespread to manage the supply and demand of energy in a dynamic way. Microgrids constitute local electrical grids consisting of distributed energy resources (DERs), such as battery energy storage systems (BESSs), photovoltaics (PVs), and inelastic or controllable loads suitably operated to achieve certain objectives. The use of control strategies is key to ensuring the optimal operation of DERs to achieve a specific objective.

Various approaches to microgrid control have been proposed in the literature [2]. Two alternative approaches are those of (i) local and grid-state myopic (e.g., droop-based [3]) and (ii) optimization-based strategies, e.g., [4,5]. We focus on the latter category, as the lack of knowledge of the grid state and the uncertainties of renewables for droop-based methods can lead to sub-optimal decisions.

We consider microgrids that have the capability to either be connected to the main grid or operate as an island. The controllability of the microgrid is provided exclusively by BESSs, whereas the rest of the energy resources are uncontrollable stochastic renewable generators and loads. Such a model is of high interest in practical applications, as BESSs are reliable and highly controllable energy sources for balancing the uncertainties of renewables [6]. We assume that the BESSs reserve part of their energy capacity to be used exclusively by the grid operator to achieve a certain objective (e.g. dispatchability). Because the batteries have a common objective, we also assume that, if the microgrid operates in islanded mode, then the role of the slack bus is not played by a BESS.

The control of the BESSs is performed in a multi-layered fashion. The higher layers target long-term energy/economic objectives and grid safety with respect to nodal voltage and branch current limits by taking into account power forecasts from uncontrollable producers and consumers. The output of these layers is typically a power profile (e.g., dispatch plan [6]) to be tracked at the bus that interfaces the microgrid with the main grid, which could be computed either a day ahead or recomputed intra-day (e.g., every 15 min) [7]. The lowest layer executes in real-time (e.g., every few seconds) the decisions made by the higher layers, whereas also taking care of grid safety as power fluctuations from their predicted values can lead the system to an undesirable state that is not accounted for in the other layers.

Assuming a given higher layer of control, we focus on the design of the optimization problem to be solved by the lowest layer. We consider a real-time layer operating at the multi-second time scale, supervised by a higher layer operating at the 15-min

* Corresponding author.
E-mail addresses: plouton.grammatikos@epfl.ch (P. Grammatikos), mario.paolone@epfl.ch (M. Paolone), jean-yves.leboudec@epfl.ch (J.-Y. Le Boudec).

https://doi.org/10.1016/j.segan.2023.101141

timescale. The objectives of the real-time layer act as proxies for the objectives of the higher layer that are difficult to express in real-time. Having no explicit guidelines for the design of the cost functions optimized by this layer might lead to an unfair usage of the BESSs in favor of a certain objective. For example, it might compromise grid safety in favor of dispatch tracking, if the two objectives are not configured carefully.

A common approach to configure the control parameters relies on the use of an "oracle" that finds the optimal set of parameters a posteriori so that acceptable performance is achieved. In other words, multiple simulations are run with different sets of weights until a satisfactory set is found. Even though this approach might work when a single grid is considered, it might not be viable in a real-life scenario because the optimal sets of weights are most likely grid and scenario dependent. Grid operators might have to configure multiple microgrids, hence they would likely have to perform an extensive series of simulations to determine the optimal set of parameters for each microgrid. Furthermore, as we show in Section 3.2, in case there is a change in the topology of a grid, or the specifications of any asset are modified, or if the boundary operating conditions are changing, the set of parameters might no longer achieve the desired performance, so the whole process would most likely have to be repeated anew.

The use of this approach can be inferred in various works in the literature. The works presented in [8–10] optimize battery state-of-charge (SoC) related penalties, in addition to the monetary cost of power generation. The cost functions used employ certain coefficients, which were chosen manually for the problem at hand, hence the problem definition does not generalize easily to other cases.

A similar approach is followed in [11]. The authors define a cost function for energy storage units, which penalizes the charging/discharging of the unit. They use a multi-agent approach to satisfy, as much as possible, all single-devices goals; they also follow a central message to meet a proposed demand. However, it is not clear how the cost functions used in the simulations are designed. The issue of objective weighing is also addressed, but the choice of the weights does not seem straightforward.

The work presented in [12] is more closely related to the problems studied in our work, as it employs a two-layer approach. It incorporates a day-ahead scheduler that computes a power profile to be followed by the intra-day scheduler while minimizing voltage deviation and power losses. The authors present a case study that examines the effect of the weights of the respective objectives, but no intuition is given behind the choice of the values.

Finally, the objectives defined in [13,14] are similar to the ones studied in our work. Each individual resource is assigned a penalty term on its active and reactive power; there is also an objective to follow a target state in the grid. However, the problem formulation includes certain weights in the objective, the choice of which is not specified.

To bridge the gap in the existing literature, we give guidelines to the design of cost functions for various objectives related to microgrids' real-time control. Our method reduces the time and effort needed to configure the parameters of the controller and gives some intuition on how it will perform a priori, without the need to run extended series of simulations. It also has the advantage of being grid and scenario independent. This means that it can be employed by grid-operators without any modifications. The problem we formulate defines two types of objectives, namely batteries and grid objectives. The purpose of the batteries' objectives are to regulate their SoC, whereas the purpose of the grid objective is to achieve a target grid state within a desired tolerance. The choice of the respective cost functions is made in such a way that the SoC trajectories of the batteries are as close as possible to each other while following the grid objective.

The structure of the paper is as follows. In Section 2, we define the optimization problem that is targeted by our control system. In Section 3, we demonstrate the problems of the oracle-based approach, using concrete examples. In Sections 4 and 5, we give the mathematical formulation of our problem that leads to the design of cost functions for batteries and grid objectives, respectively. In Section 6, we validate our theoretical analysis with simulations. Finally, in Section 7, we conclude the paper.

2. General form of the optimization objective

We consider a microgrid connected to the main grid to be controlled by N batteries that can implement any active/reactive power setpoint $\boldsymbol{x}_i = (P_i, Q_i) \in \mathcal{A}_i, i = 1..N$, where $\mathcal{A}_i$ is the constraint set of battery i. The grid also consists of U uncontrollable energy resources of uncertain prosumption $\boldsymbol{u}_n = (\mathcal{P}_n, \mathcal{Q}_n), n = 1..U$. The optimal power setpoints for each battery are computed periodically by a centralized controller that is assumed to have knowledge of the SoC of each battery (SoC_i) and the state of the grid. The theoretical analysis presented in this work is independent of the period of the control, which can take values in the minute down to the sub-second scale. Therefore, our goal is to design an optimization problem that can be solved efficiently, meaning that (i) it should be convex and (ii) the number of hard constraints should be limited.

Each battery has a cost function, called *battery objective*, related to it; it indicates its preference to implement a specific point within its constraint set. We indicate with $C_i(\boldsymbol{x}_i|S_i, SoC_i)$ the cost function of battery i, where S_i is the rated apparent power of its power-electronic converter. In addition to the individual battery objectives, the controller should also aim to achieve a target grid state with respect to (i) the power at the point of common coupling (PCC), i.e. the point that connects the microgrid to the external grid, (ii) nodal voltages, and (iii) branch currents. We call this the *grid objective*, denoted as $J(\boldsymbol{x}|\hat{\boldsymbol{u}})$, where $\boldsymbol{x} = (\boldsymbol{x}_1, \boldsymbol{x}_2, \ldots, \boldsymbol{x}_N)$ is the set of batteries setpoints and $\boldsymbol{u} = (\boldsymbol{u}_1, \boldsymbol{u}_2, \ldots, \boldsymbol{u}_U)$ is the set of the prosumptions of the uncontrollable resources. The objective of the controller at every time step t is to minimize the total expected cost, subject to the batteries' constraints.

$$\min_{\boldsymbol{x}} C_t(\boldsymbol{x}|\hat{\boldsymbol{u}}) \ , s.t. \ \boldsymbol{x}_i \in \mathcal{A}_i, i = 1..N \tag{1}$$

$$C_t(\boldsymbol{x}|\boldsymbol{u}) = \sum_{i=1}^{N} C_i(\boldsymbol{x}_i|S_i, SoC_i) + J(\boldsymbol{x}|\boldsymbol{u}) \tag{2}$$

where $\hat{\{\cdot\}}$ denotes the forecast of the prosumption. In this formulation, hard grid-constraints concerning nodal-voltage deviations, ampacity limits, or power factors can either be relaxed to soft constraints or be expressed via appropriate cost functions [15].

Concerning the convexity of problem (1), the cost functions of the batteries and their respective constraint sets can easily be designed to be convex. However, in the case of the grid objective, some approximations are needed due to the well-known non-convex characteristics of the power-flow equations.

We consider that we want to optimize the value of M grid variables $\boldsymbol{y} = (y_1, y_2, \ldots, y_M)$, where y_m can represent a specific nodal injection, nodal voltage, or branch current. For this purpose, we consider grid cost-functions of the following form:

$$J(\boldsymbol{x}|\boldsymbol{u}) = \sum_{m=1}^{M} w_m J_m(y_m(\boldsymbol{x}|\boldsymbol{u})) \tag{3}$$

where J_m is the penalty term for the grid variable y_m and $w_m > 0$ is the respective weight.

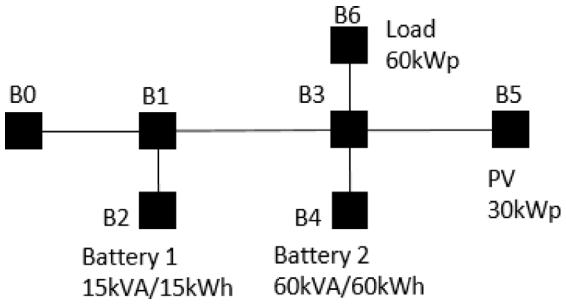

Fig. 1. Microgrid topology. B0 is the slack bus.

The power-flow equations link the complex power injections with the nodal voltages in the following way [16]:

$$\bar{S}_k = \bar{E}_k \sum_{k'=1}^{K} \underline{Y}_{kk'} \underline{E}_{k'} \tag{4}$$

where K is the number of buses in the grid, $\bar{E}_k, \bar{S}_k$ denote the complex voltage and power injection of bus k, $\bar{Y}$ is the nodal admittance matrix and $\{\cdot\}$ indicates the complex conjugate. Because of the form of Eq. (4), the relation between voltages, currents, and active/reactive power is non-convex. One way to achieve convexity is to use a linear approximation of (4), using, for example, the method presented in [16]. Using the notation presented earlier in this section, we approximate the grid variable y_m at time t, as follows:

$$\begin{aligned} y_m(\boldsymbol{x}|\boldsymbol{u}) = y_m^0 + \sum_{i=1}^{N} (K_{P,i}^m (P_i - P_i^0) + K_{Q,i}^m (Q_i - Q_i^0)) + \\ + \sum_{n=1}^{U} (K_{\mathcal{P},n}^m (\mathcal{P}_n - \mathcal{P}_n^0) + K_{\mathcal{Q},n}^m (\mathcal{Q}_n - \mathcal{Q}_n^0)) \end{aligned} \tag{5}$$

where y_m^0, P_i^0 and Q_i^0 are the values of y_m, P_i and Q_i respectively at time $t-1$ and $K_{P,i}^m$, $K_{Q,i}^m$ are the so-called *sensitivity coefficients*, with respect to the batteries setpoints. Accordingly, $\mathcal{P}_n^0$, $\mathcal{Q}_n^0$ are the values of the uncontrollable prosumptions at $t-1$ and $K_{\mathcal{P},n}^m$, $K_{\mathcal{Q},n}^m$ are the respective sensitivity coefficients. The sensitivity coefficients represent precisely the partial derivatives of the grid variable with respect to the nodal powers evaluated at the value of the setpoints at time $t-1$.

3. The oracle-based approach

The need for having guidelines for the design of cost functions is demonstrated on the microgrid of Fig. 1. It is composed of two uncontrollable prosumers, namely a PV plant of 30 kWp and a load of 60 kWp; both of which have a power factor of 0.9. It also contains two controllable batteries, namely battery 1 rated at 15 kVA/15 kWh, and battery 2 rated at 60 kVA/60 kWh. The parameters of the grid lines are in [17].

We assume a control system in three layers. The first layer, called the *day-ahead layer*, receives as an input (i) the SoC of the two batteries at the beginning of the day and (ii) scenario-based, day-ahead forecasts of the PV generation and load consumption at a 5-minute resolution for a horizon of 24 h. Then, it computes a dispatch plan, as well as the expected trajectory of the SoC of each battery for each scenario, using the method of [18]. Because the forecasts that are performed day-ahead are typically inaccurate, every 15 min a re-dispatching is performed by an *intra-day layer* that updates the dispatch plan and/or SoC trajectories of the batteries using updated forecasts for the prosumption. Finally, we

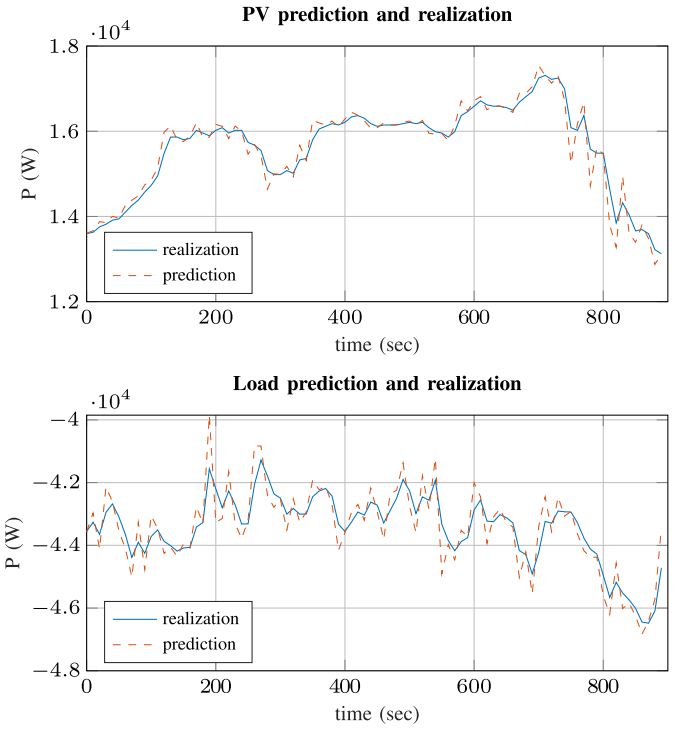

Fig. 2. Predictions and realizations of the uncontrollable energy resources in the microgrid of Fig. 1.

consider a time slice of 15 min between two intra-day cycles for the *real-time layer*. We solve problem (1) every 10 s, assuming given point-forecasts of the prosumption at a 10 s horizon generated by a second forecasting model. It should be noted that the intra-day and the real-time forecasters are assumed to be independent. Therefore, we can consider only the real-time forecasts to solve problem (1). Fig. 2 shows the real-time realization of the PV generation and load consumption for the considered 15 min interval and their respective real-time forecasts.

3.1. Cost functions

The target SoC trajectory, $SoC_{DP,i}$, for battery i is taken as the median trajectory over all scenarios computed by the intra-day layer. The cost function proposed in [19], so that battery i ($i = \{1, 2\}$) achieves this target SoC, is the following[1]:

$$\begin{aligned} &C_i(P_i, Q_i|S_i, SoC_i) = \\ &\quad w_i \frac{|\Delta SoC_i|}{3} \left(\frac{P_i^2}{S_i^2} - 2sgn(\Delta SoC_i)\frac{P_i}{S_i}\right) \end{aligned} \tag{6}$$

where $\Delta SoC_i = SoC_i - SoC_{DP,i}$ is the difference between the SoC of the battery and the target value normalized in the interval $[-1, 1]$. $w_i > 0$ is the weight placed on the objective of battery i, which is to be configured by the user. For simplicity, we use the following linear approximation of the constraint set of the batteries' power-electronics converters: $P_i, Q_i \in [-\frac{\sqrt{2}}{2}S_i, \frac{\sqrt{2}}{2}S_i]$.

The grid objective consists of the following four objectives: (i) track an active power profile at the microgrid slack bus, (ii) minimize the reactive power at the slack bus, (iii) minimize the nodal-voltage deviations from the nominal value, (iv) limit the branch currents.

[1] The rationale behind this function is the following: if $SoC_i < SoC_{DP,i}$ then the function is increasing with respect to P_i, thus favoring charging of the battery (negative power) instead of discharging. If, on the other hand, $SoC_i > SoC_{DP,i}$, then the function is decreasing, so that it favors discharging of the battery.

The cost functions we use in this work are adapted from [14]. Objectives (i) and (ii) can be expressed with the following two equations, respectively:

$$J_{P_s}(\boldsymbol{x}|\boldsymbol{u}) = (P_s(\boldsymbol{x}|\boldsymbol{u}) - P_{DP})^2 \tag{7}$$

$$J_{Q_s}(\boldsymbol{x}|\boldsymbol{u}) = Q_s^2(\boldsymbol{x}|\boldsymbol{u}) \tag{8}$$

where (P_s, Q_s) are the linearized active and reactive powers at the slack bus, computed from (5), and P_{DP} is the active power tracking value computed by the dispatch plan.

To express objective (iii), we assume a single node k with linearized voltage magnitude V_k and define the hard voltage constraint, denoted as β_{hard}. This objective should ensure that V_k does not differ more than β_{hard} units from the nominal value V_n. Therefore, the cost function should take very large values for $|V_k - V_n| > \beta_{hard}$. The cost function for voltage V_k can be defined in the range $|V_k - V_{nom}| \leq \beta_{hard} - \epsilon$, where $0 < \epsilon \ll \beta_{hard}$ as [19]:

$$J_{V_k}(\boldsymbol{x}|\boldsymbol{u}) = \frac{(V_k(\boldsymbol{x}|\boldsymbol{u}) - V_{nom})^2}{\beta_{hard}^2 - (V_k(\boldsymbol{x}|\boldsymbol{u}) - V_{nom})^2} \tag{9}$$

The constant ϵ prevents the function from taking infinite values. Outside this range, the cost is defined as a quadratic cost function of V_k such that $J_V(V_k)$ and $J'_V(V_k)$ are both continuous at $V_k = V_{nom} \pm (\beta_{hard} - \epsilon)$.

The purpose of objective (iv) should be to keep the magnitude of the linearized complex current $\bar{I}_l$ of line l below its ampacity I_l^{max}. Unlike the voltages, however, the magnitude of branch currents cannot always be accurately approximated as a linear function of nodal powers. Instead, we can first approximate the constraint $|\bar{I}_l| \leq I_l^{max}$ by the following linear constraints:

$$\begin{aligned} I_l^+ &\geq -I_l^{max} \\ I_l^- &\leq I_l^{max} \end{aligned} \tag{10}$$

where $I_l^+ = \Re(\bar{I}_l) + \Im(\bar{I}_l)$ and $I_l^- = \Re(\bar{I}_l) - \Im(\bar{I}_l)$ and $\Re(\cdot), \Im(\cdot)$ indicate the real and imaginary part. We can then represent constraints (10) in the range $\frac{I_l^{+/-}}{I_l^{max}} \leq 1 - \epsilon$ using two penalty terms per line, as in [19]:

$$J_{I_l^{+/-}}(\boldsymbol{x}|\boldsymbol{u}) = \frac{(I_l^{+/-}(\boldsymbol{x}|\boldsymbol{u}))^2}{(I_l^{max})^2 - (I_l(\boldsymbol{x}|\boldsymbol{u})^{+/-})^2} \tag{11}$$

The cost is defined again outside this range as a quadratic function, such that $J_I(I_l^{+/-})$ and $J'_I(I_l^{+/-})$ are both continuous at $I_l^{+/-} = (1-\epsilon)I_l^{max}$.

The total grid cost function is the following:

$$\begin{aligned} J(\boldsymbol{x}|\boldsymbol{u}) &= w_s(J_{P_s}(\boldsymbol{x}|\boldsymbol{u}) + J_{Q_s}(\boldsymbol{x}|\boldsymbol{u})) + \\ &+ \frac{w_V}{K}\sum_{k=1}^{K} J_{V_k}(\boldsymbol{x}|\boldsymbol{u}) + \frac{w_I}{L}\sum_{l=1}^{L} J_{I_l^+}(\boldsymbol{x}|\boldsymbol{u}) + J_{I_l^-}(\boldsymbol{x}|\boldsymbol{u}) \end{aligned} \tag{12}$$

where K is the number of buses, L is the number of lines and $w_s, w_V, w_I > 0$ are user-defined weights.

3.2. Simulation results

We perform simulations over a period of 15 min with a time interval of 10 s between the computation of setpoints. To evaluate the effectiveness of the controller in balancing the various objectives, we study an extreme case where the slack voltage drops below the nominal value (see Fig. 3). The simulations are performed in MATLAB and the problem is solved using the interior-point method implemented by the *fmincon* function.

Considering the cost functions defined above, it is up to the user to properly choose the weights of the objectives. We first consider using the same weight for all objectives: $w_s = w_V = w_I = w_1 = w_2 = 1$. Looking at the simulation results shown in Fig. 3, we notice that the slack can neither track the dispatch plan (see active power plot) nor effectively control its reactive power (green line in the reactive power plot), even though there is enough controllability in the batteries to do so. Indeed, the powers and SoCs of the batteries, as well as the nodal voltages and branch currents, are all well within their respective bounds. In particular, voltage magnitudes are within 4% of the nominal value and all currents are below 50% of the respective line ampacities. Looking at the active-powers graph, we notice that the batteries discharge for the majority of the simulation, even though this is contrary to their own objective and that of the tracking. The reason is that the controller tries to increase the voltages as much as possible, which means that the weight w_s is too small compared to the weight w_V, as we will verify next.

This simulation indicates that the chosen cost functions do not lead to a balanced satisfaction of the objectives. For the next simulation, we consider adapting the weights of the objectives, to achieve a more balanced control. The choice is made as follows: we first fix the slack weight $w_s = 1$. Then, we run simulations with varying weights for the rest of the objectives, such that (i) the slack tracks the dispatch plan with an acceptable accuracy (ii) the controller's reaction to the voltage drop is less significant and (iii) the batteries SoC are close to the target trajectories. After a series of simulations, we settle with the weights $w_s = 1$, $w_V = 10^{-5}$, $w_I = 10^{-4}$, $w_1 = 10^{-4}$ and $w_2 = 5 \cdot 10^{-4}$.

The simulation results are shown in Fig. 4. First of all, all voltages and currents are still kept within their respective bounds. However, there are certain major improvements to be observed, compared to Fig. 3. Concerning the active power, the controller does a much better job at tracking the dispatch plan, while the reactive power injection to the external grid is kept close to 0. Regarding the SoC graph, we observe a more fair regulation between the two batteries. Even though at the beginning of the day there is a mismatch between the two lines due to the voltage drop, then they follow a similar trajectory. More specifically, the maximum relative deviation between the two lines is only 0.2%, as opposed to 3% in Fig. 3 (notice that the scales in the y-axis are different for the two plots).

We now consider the following scenario. The grid operator purchases a new battery with the same specifications as Battery 2, i.e. at 60 kVA/60 kWh and replaces the old Battery 1 with this new battery. The line between B1–B2 is also reinforced with a new one with four times the ampacity to ensure that it can withstand the current drawn by the new battery. Because there is a change in the grid, the first step is to re-compute a dispatch plan, as explained at the beginning of Section 3. We assume that the grid operator has already computed the weights $w_s = 1$, $w_V = 10^{-5}$, $w_I = 10^{-4}$, $w_1 = 10^{-4}$ and $w_2 = 5 \cdot 10^{-4}$, so they consider using the same ones for this new grid. Therefore, we re-run the simulation with this change in the grid and the same weights as before.

The results are shown in Fig. 5. The main difference can be observed in the SoC trajectories of the two batteries. Unlike Fig. 4, the two SoCs follow different directions throughout this 15 min simulation. More precisely, although the maximum percentage difference between the two SoCs was 0.2% in Fig. 4, it has now increased to 1%. Also, this difference is expected to become more prominent in a longer time-period, as the two batteries follow opposite trajectories.

This example was used to showcase that the optimal set of weights is typically grid-dependent. Therefore, each change in the grid would require repeating the weight-tuning process anew, which can be a tedious and time-consuming process, especially

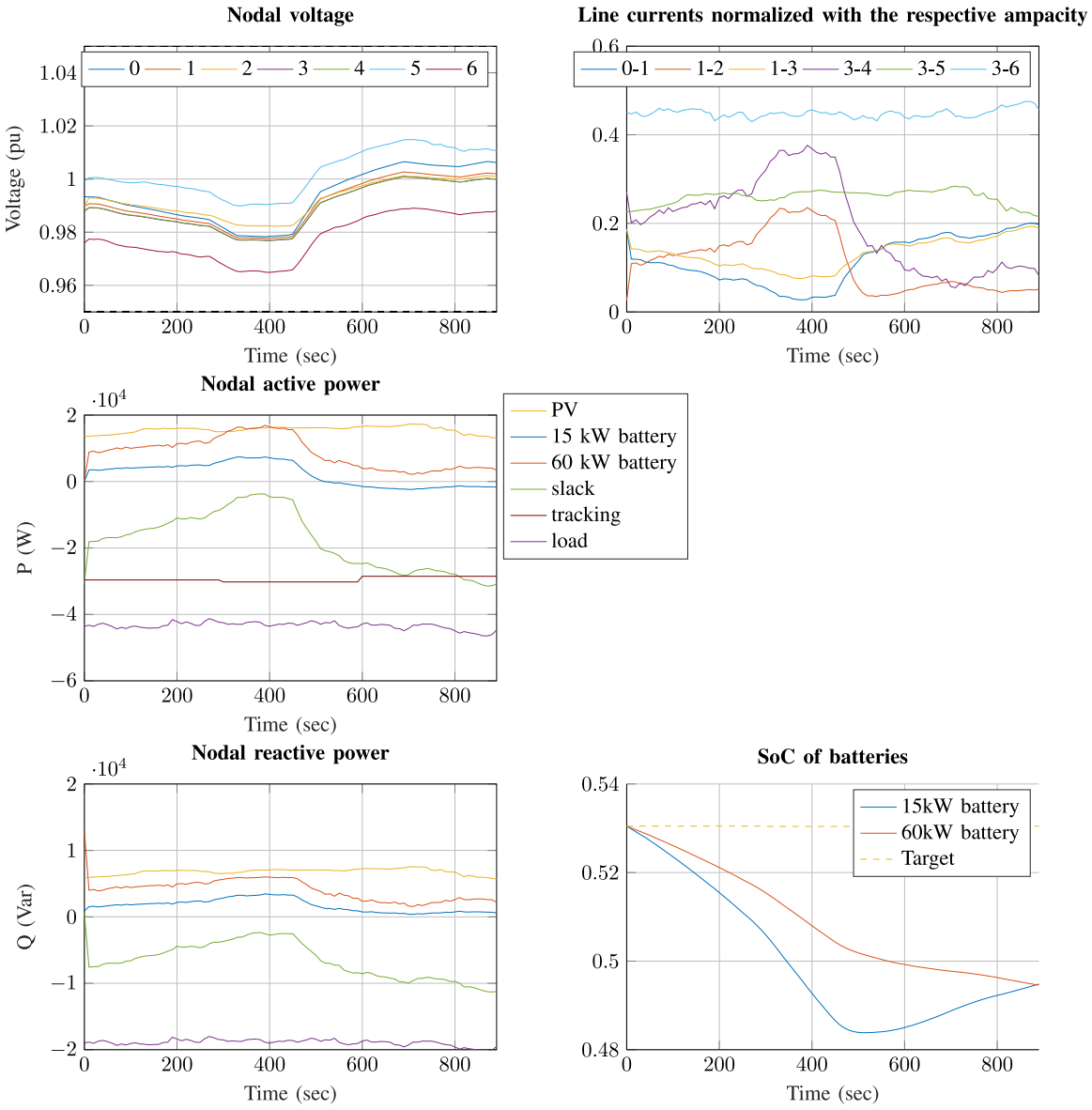

Fig. 3. Simulation results with equal weights for all objectives. The bottom-right graph shows the target trajectory for the SoC of the batteries that was computed by the intra-day layer of control.

in larger grids. In addition, a grid operator would have to execute the same process for each grid they operate, in case they are responsible for multiple grids.

To address the problem, we formalize a method to construct the cost functions in (2) so that we do not need to configure any parameters a posteriori. The values of the parameters of the cost functions should be chosen in an intuitive manner so that the behavior of the controller can be predicted a priori.

4. Battery cost-function

4.1. Fair control of batteries

The battery objectives should be chosen in such a way that a fair control among them is achieved in order to follow the grid objective. Although various definitions of fairness can be used, we choose one that applies to short-term objectives.

Battery Design Goal and Preference of Batteries: We assume that a higher layer of control has computed a point

$$\boldsymbol{x}_i^*(SoC_i) = (P_i^*(SoC_i), Q_i^*(SoC_i)) \in [-\frac{S_i}{\sqrt{2}}, \frac{S_i}{\sqrt{2}}] \times [-\frac{S_i}{\sqrt{2}}, \frac{S_i}{\sqrt{2}}]$$

for battery i, called the *preference* of the battery. It is the point that the battery should implement if the grid does not impose any other constraints. Taking the example of Section 3.1, the preference would be the power setpoint that brings the SoC of the battery as close to the target value as possible.

However, because there might be conflicting objectives on the grid, the batteries might not be able to simultaneously implement their preference. The deviation of a battery's implementation

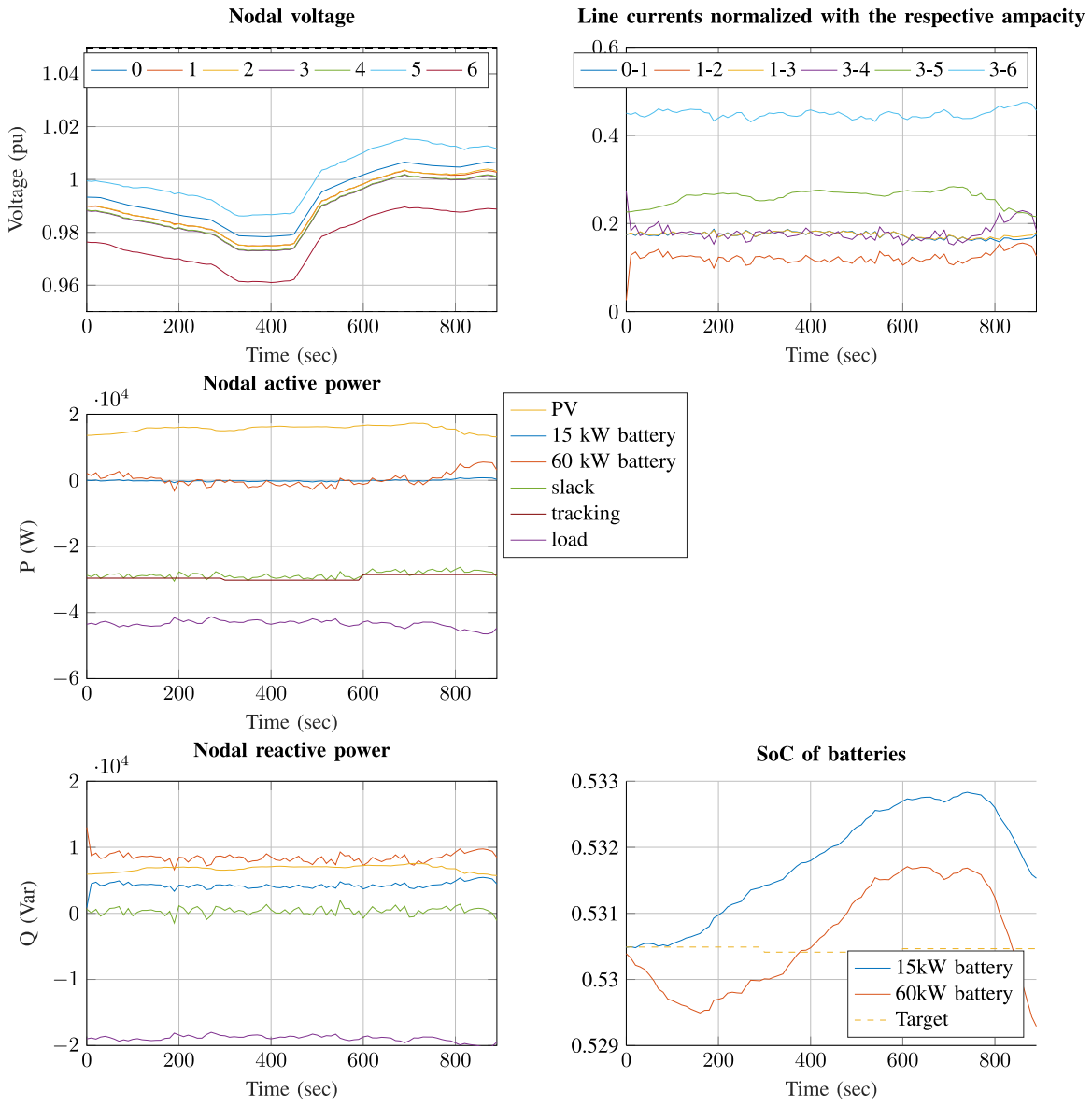

Fig. 4. Simulation results with manually picked weights: slack weight $w_s = 1$, voltage weight $w_V = 10^{-5}$, current weight $w_I = 10^{-4}$, battery weights $w_1 = 10^{-4}$, $w_2 = 5 \cdot 10^{-4}$.

from its preference can be measured using its *preference ratios* that, with respect to P and Q, are defined as:

$$r_{P,i} = \frac{P_i^{opt} - P_i^*}{S_i}, r_{Q,i} = \frac{Q_i^{opt} - Q_i^*}{S_i} \tag{13}$$

where (P_i^{opt}, Q_i^{opt}) is the solution of problem (1) for battery i.

One possible choice for a fairness condition would be an equal preference ratio for all batteries. A similar definition is given in [20]. However, in our case this might not be the best choice, considering that the grid objective is also involved. Instead, we take as *fairness* the condition where the preference ratio of a battery is proportional to the effect this battery has on minimizing the grid objective. Formally, our fairness condition is $\forall i = 1..N$:

$$r_{P,i} = \lambda_P \frac{\partial J(\boldsymbol{x}^{opt}|\hat{\boldsymbol{u}})}{\partial P_i}, r_{Q,i} = \lambda_Q \frac{\partial J(\boldsymbol{x}^{opt}|\hat{\boldsymbol{u}})}{\partial Q_i} \tag{14}$$

where the coefficients λ_P and λ_Q are the same for all batteries.

This means that batteries that can easily affect the grid objective should be exploited for this purpose, assuming that this is achievable by the battery's capabilities, even if this contradicts their own preference. Whereas, if the choice of the power setpoint for a specific battery does not affect the grid objective, then we can freely choose to satisfy the preference of the battery.

4.2. General form of a battery cost function

We assume that each battery has two separate objectives, specifically (i) satisfy its preference and (ii) minimize the internal losses of the power interface that interconnects the battery with the grid. The first objective can be met by steering the stationary point of the cost, whereas the second can be achieved with the addition of a quadratic penalty function of the active and reactive powers. Therefore, we consider the following cost function for battery i:

$$\begin{aligned} C_i(P_i, Q_i|S_i, SoC_i) = a_P\left(\frac{P_i^2}{4S_i} - \frac{P_i^*(SoC_i)}{2S_i}P_i\right) + \\ + a_Q\left(\frac{Q_i^2}{4S_i} - \frac{Q_i^*(SoC_i)}{2S_i}Q_i\right) + c \end{aligned} \tag{15}$$

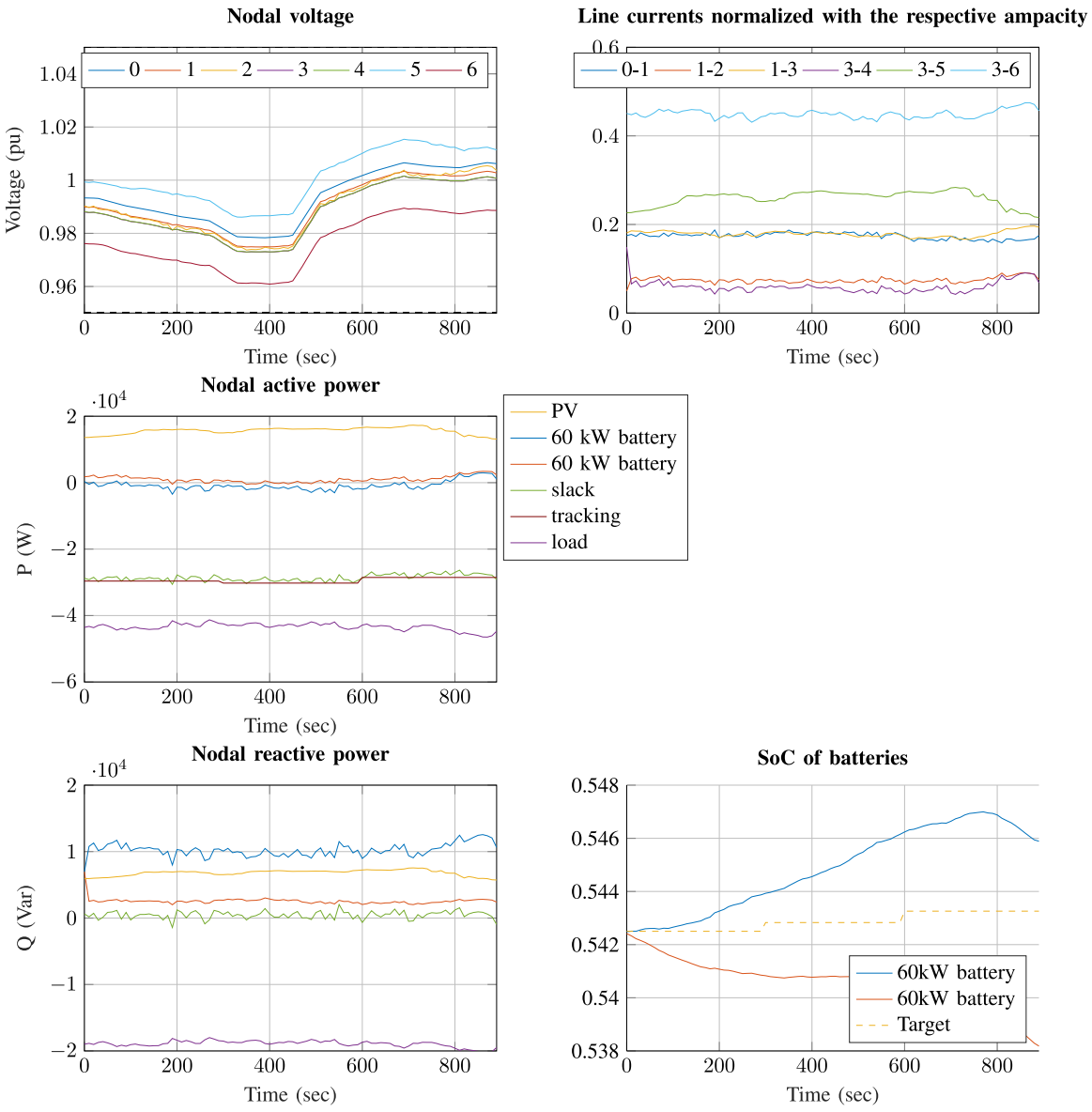

Fig. 5. Simulation results with manually picked weights and a bigger Battery 1 at 60 kVA/60 kWh.

where a_P, a_Q are strictly positive so that the function is strictly convex and c is any arbitrary constant.[2] By defining the function this way, one can verify that the point that minimizes it is precisely the preference of the battery. Theorem 1 shows that this cost function satisfies our definition of fairness under certain conditions.

Theorem 1. *We consider the unconstraint variant of problem (1), i.e. with $\mathcal{A}_i = \mathbb{R}^2$, $i = 1..N$ where the cost function for all N batteries is defined in (15). Then the optimal solution of the problem satisfies conditions (14) with $\lambda_P = -\frac{2}{a_P}$ and $\lambda_Q = -\frac{2}{a_Q}$.*

The proof of this theorem, as well as all other theorems and lemmas are provided in the appendix. Theorem 1 states that fairness is guaranteed provided that the batteries have unconstrained setpoints. We now study how much we can deviate from ideal fairness, when the battery constraints are involved, in the following scenario: we consider two batteries $i, j \in \{1, \dots, N\}$ that (i) have the same preference, normalized by the rated power:

$$\frac{\boldsymbol{x}_i^*(SoC_i)}{S_i} = \frac{\boldsymbol{x}_j^*(SoC_j)}{S_j} \tag{16}$$

and (ii) have the same constraints, normalized by the rated power, which are in the following form, for $m \in \{i, j\}$:

$$\begin{aligned} \frac{P_m}{S_m} &\in [(\frac{P}{S})_{min}, (\frac{P}{S})_{max}] \\ \frac{Q_m}{S_m} &\in [(\frac{Q}{S})_{min}, (\frac{Q}{S})_{max}] \end{aligned} \tag{17}$$

It should be noted that it is reasonable to assume that conditions (16) and (17) are satisfied simultaneously, because (i) batteries that have the same constraints should have the same objective and (ii) the preference can be designed in such a way that the conditions are satisfied. Theorem 2 is a generalization of Theorem 1, when the binding constraints of the batteries are considered.

Theorem 2. *We consider problem (1), where the cost function for all N batteries is defined in (15). We also consider two batteries*

[2] It should be noted that the value of c does not affect the solution of the optimization problem (1).

$i, j \in \{1, \ldots, N\}$, for which conditions (16) and (17) are true. Then the solution of optimization problem (1) satisfies the following conditions:

$$|r_{P,i} - r_{P,j}| \leq \frac{2}{a_P} \left| \frac{\partial J(\boldsymbol{x}^{opt}|\hat{\boldsymbol{u}})}{\partial P_i} - \frac{\partial J(\boldsymbol{x}^{opt}|\hat{\boldsymbol{u}})}{\partial P_j} \right| \tag{18}$$

$$|r_{Q,i} - r_{Q,j}| \leq \frac{2}{a_Q} \left| \frac{\partial J(\boldsymbol{x}^{opt}|\hat{\boldsymbol{u}})}{\partial Q_i} - \frac{\partial J(\boldsymbol{x}^{opt}|\hat{\boldsymbol{u}})}{\partial Q_j} \right| \tag{19}$$

where $r_{P,m}, r_{Q,m}, m \in \{i, j\}$ are defined in (13). The upper bound is achieved under the assumptions of Theorem 1.

Theorem 2 states that the conditions of Theorem 1 are sufficient to achieve the upper bound of the differences $|r_{P,i} - r_{P,j}|$ and $|r_{Q,i} - r_{Q,j}|$. This means that adding constraints to the problem will definitely reduce the difference of the preference ratios compared to the unconstrained case. Because the upper bounds of conditions (18) and (19) correspond to our definition of fairness (condition (14)), the worst case, in terms of fairness, is the one where the preference ratios are equal. Therefore, cost function (15) always achieves a state between our fair condition and the one used in [20]. Moreover, the theorem gives some intuition on the effect that the coefficients a_P, a_Q have on the fairness between the two batteries. It shows, in particular, how increasing the weights of the cost terms causes an inversely proportional decrease in the difference between the respective preference ratios.

5. Grid objective

The purpose of the grid objective is to achieve a target grid state. Assuming grid cost-functions in the form (3), we define the *preference* y_m^* of grid variable y_m, as $y_m^* = \arg\min_{y_m} J_m(y_m)$. In many practical applications, a deviation Δy_m from the target value y_m should be penalized the same as a deviation $-\Delta y_m$. In this case, we require that J_m is in the following form:

$$J_m(y_m) = J_m^*(y_m - y_m^*) \tag{20}$$

where $J_m^*(y)$ is a strictly convex, even function of y.

5.1. Computing the weights w_m

We propose a method for choosing the weight w_m of objective J_m that is independent of the state of the batteries connected to the grid. We assume that we use a cost function of the form (15) for every battery, and we choose the coefficients a_P, a_Q, such that $0 < a_P, a_Q < 1$.

Grid Design-Goal: A typical purpose of any grid objective J_m would be to keep the difference of grid variable y_m from its target value y_m^* within a specified bound $d_{max,m}^*$. Therefore, the weight w_m should be chosen, such that

$$|y_m^{opt} - y_m^*| \leq d_{max,m}^* \tag{21}$$

where $y_m^{opt} = y_m(\boldsymbol{x}^{opt}|\hat{\boldsymbol{u}})$ is the value of y_m when the optimal solution of problem (1) is implemented. Lemma 1 computes an upper bound for $|y_m^{opt} - y_m^*|$ as a function of the weight w_m, which will be proven useful in achieving condition (21).

Lemma 1. *We assume a grid cost-function of the form: $J(\boldsymbol{x}|\boldsymbol{u}) = J_m(y_m(\boldsymbol{x}|\boldsymbol{u}))$ where $J_m(y_m)$ is a strictly convex function of the grid variable y_m that is expressed in the form (5). We also assume that the constraints of the batteries are in the form $x_i \in [x_{i,min}, x_{i,max}], \forall i = 1..N$, where $x_i = \{P_i, Q_i\}$. We define the following functions:*

$$K_t(w_m, d) = \frac{1}{w_m J_m'(y_m^* + d)} \tag{22}$$

$$h(K) = |y_m^* - y_m^{inf}| + \sum_{|K_{x,i}^m| < K} |K_{x,i}^m||x_{i,max} - x_{i,min}| \tag{23}$$

$$g(w_m, d) = \max\{d, h(K_t(w_m, d))\} \tag{24}$$

$$f(w_m) = \min_{d>0} g(w_m, d) \tag{25}$$

where w_m is the weight of objective $J_m(y_m)$, $J_m'(y_m)$ is the derivative of J_m with respect to y_m and y_m^{inf} is the point that minimizes J_m within its domain, i.e.

$$y_m^{inf} = \arg\min_{y_m \in [y_m^{min}, y_m^{max}]} J_m(y_m) \tag{26}$$

Then, the function $f(w_m)$ is an upper bound of $|y_m^{opt} - y_m^*|$.

It should be noted that functions K_t, h and g defined in (22), (23) and (24) respectively are just auxiliary functions that help in the proofs of the theorems and the visualization of the upper bound, as shown in Section 5.3. K_t can be interpreted as a threshold, under which the values of the sensitivities are negligible in computing the upper bound for $|y_m^{opt} - y_m^*|$.

Lemma 1 gives an upper bound for the quantity $|y_m^{opt} - y_m^*|$ as a function of the weight w_m. However, the actual realization y_m^{real} will differ from the optimal value y_m^{opt}, because of the uncertainty in the system, as follows:

$$y_m^{real} = y_m^{opt} + \Delta y_m \tag{27}$$

$$\Delta y_m = \sum_{n=1}^{U} (K_{\mathcal{P},n}^m \Delta \mathcal{P}_n + K_{\mathcal{Q},n}^m \Delta \mathcal{Q}_n) \tag{28}$$

where $\Delta \mathcal{P}_n$, $\Delta \mathcal{Q}_n$ are the uncertainties of prosumption n, i.e. the difference between the forecast value and the respective realization, and $K_{\mathcal{P},n}^m$, $K_{\mathcal{Q},n}^m$ are the sensitivity coefficients of y_m with respect to the nodal prosumption (see Section 2 and [16]).

Theorem 3 generalizes the statement of Lemma 1, by computing an upper bound for the quantity $|y_m^{real} - y_m^*|$ as a function of the objective's weight w_m. The theorem, therefore, accounts for the uncertainty in the system.

Theorem 3. *Given the same assumptions as Lemma 1 and Eq. (27), then*

$$|y_m^{real} - y_m^{opt}| \leq f(w_m) + |\Delta y_m|_{max} \triangleq f_u(w_m) \tag{29}$$

where $|\Delta y_m|_{max} = \max_{\mathcal{P}_n, \mathcal{Q}_n} |\Delta y_m|$ is the maximum absolute uncertainty of y_m due to the forecast errors and $f(w_m)$ is given by (25).

Although, the reverse problem interests us, specifically, given a desired upper bound $d_{max,m}^*$, we need to compute:

$$\min w_m > 0 \text{ such that } f_u(w_m) \leq d_{max,m}^* \tag{30}$$

Even though numerical methods can be used to approximate the solution of problem (30), we demonstrate below that we can find an analytical solution to the problem. To do this, we need to use the following properties of $f_u(w_m)$.

(1) It is a decreasing function of w_m.
(2) It has an upper bound
$$f_{UB} = |y_m^* - y_m^{inf}| + \sum_{\forall i} |K_{x,i}^m||x_{i,max} - x_{i,min}| + |\Delta y_m|_{max}$$
(3) It has a lower bound $f_{LB} = |y_m^* - y_m^{inf}| + |\Delta y_m|_{max}$
(4) If $f_{LB} \neq 0$, then $f_u(w_m) = f_{LB}, \forall w_m \geq \frac{1}{|K^m|_{min}|J_m'(y_m^{inf})|}$ where $|K^m|_{min} = \min |K_{x,i}^m|$

The statement of Theorem 4 is used to analytically find the solution of problem (30).

Theorem 4. *We consider the following two problems,* ***Problem 1*** *given by (30) and* ***Problem 2*** *given by (31):*

$$\begin{aligned} &\min w_m > 0 \text{ such that} \\ &g(w_m, d^*_{max,m} - |\Delta y_m|_{max}) \leq d^*_{max,m} - |\Delta y_m|_{max} \end{aligned} \tag{31}$$

If w^*_m is the solution to Problem 2 (if it exists), then it is also the solution to Problem 1.

Theorem 4 states that to find the solution of the original Problem 1, we could instead solve the equivalent Problem 2. The value of this statement lies in the fact that the constraint of Problem 2 can be easily evaluated, unlike the constraint of Problem 1. Indeed, given the definitions of functions g and h one can see that the function $g(w_m, d^*_{max,m} - |\Delta y_m|_{max})$ is a step-value function of w_m, while on the other hand $f_u(w_m)$ is a complicated, smooth function. This means that only a finite number of evaluations is needed to compute the optimal weight. Considering Theorem 4 and the properties of $f(w_m)$ given above, we have the following formula for computing w_m:

$$w_m = \begin{cases} 0 & \text{if } d^*_{max,m} > f_{UB} \\ \frac{1}{|K^m|_{min}|J'_m(y^{inf}_m)|} & \text{if } d^*_{max,m} < f_{LB} \\ \frac{1}{K^m_t|J'_m(y^*_m + d^*_{max,m} - |\Delta y_m|_{max})|} & \text{else} \end{cases} \tag{32}$$

where $K^m_t = \max K$ such that $h(K) < d^*_{max,m}$. The explanation is the following: if the desired upper bound $d^*_{max,m}$ is larger than the upper bound of f_u, then we can freely choose $w_m = 0$, as any weight would satisfy the desired upper bound. Whereas, if it is lower than the lower bound of f_u, then Problems 1 and 2 cannot be solved, so we choose the maximum possible value of the weight. In any other case, Theorem 4 applies, so we can compute the weight by solving Problem 2. The solution is trivial as $g(w_m, d)$ takes only a finite number of values for a given d.

Concerning the complexity of computing the weight, formula (32) requires at most evaluating the function J'_m at a given point and computing either the minimum or the maximum value of the sensitivity coefficients of grid variable y_m. The number of sensitivities of one grid variable scales linearly with the number of buses, so the complexity of the method for one grid objective is $\mathcal{O}(K)$, where K is the number of buses in the grid. If M grid variables are considered, then the complexity of the method is $\mathcal{O}(M \cdot K)$.

The properties of $f_u(w_m)$ also give a rule for choosing $d^*_{max,m}$. According to the definition of $f_u(w_m)$, it is obvious that $d^*_{max,m}$ should not be smaller than $|\Delta y_m|_{max}$, otherwise the problem (30) will be infeasible. Therefore, we should ensure that $d^*_{max,m} > |\Delta y_m|_{max}$. In low-voltage grids, we can assume that the values of the sensitivities do not significantly change within slices of 15 min. Therefore, we can approximate the value of $|\Delta y_m|_{max}$ by using the values of the sensitivities at the beginning of the 15-min interval.

5.2. Application to specific grid objectives

We now examine how the weight computation method presented in Section 5.1 can be applied to the grid objectives defined in Section 3.1. All grid cost-functions considered so far can be expressed in the form (20), hence their weights can be computed using Theorems 3 and 4.

The target values of the slack objectives (7) and (8) are $P^*_s = P_{DP}$ and $Q^*_s = 0$. The respective desired upper bounds, used to compute the weights w_{P_s} and w_{Q_s}, can be interpreted as $d^*_{max,P_s} = |P_s - P_{DP}|_{max}$ and $d^*_{max,Q_s} = |Q_s|_{max}$, i.e. they are the maximum desired dispatch tracking difference and maximum slack reactive power respectively.

Concerning the voltage objective (9), we define, in addition to the hard voltage constraint β_{hard}, the soft voltage constraint β_{soft}. The soft voltage constraint guarantees that V_k will not deviate more than β_{soft} from the nominal voltage V_n assuming that the assumptions of Theorem 3 are true. Therefore, it can be used to compute the weight of the objective with $V^*_k = V_{nom}$ and $d^*_{max,V_k} = \beta_{soft}$.

Similarly, for the current objective, we define the soft current constraint for line l as $I^{soft}_l = \gamma_{soft} I^{max}_l$, where $\gamma_{soft} \in (0, 1-\epsilon)$ is a given constant that defines a soft upper bound for each line. This bound can be used to compute the weights w_{I_l}, with $(I^{+/-}_l)^* = 0$ and $d^*_{max,I^{+/-}_l} = I^{soft}_l$.

5.3. Visual representation of the computed upper bound

To help us visualize the results from the past sections, we consider an instance of the grid shown in Fig. 1. The preference of each battery (according to Definition 1) is $\boldsymbol{x}^*_i = (S_i\ (W), 0\ (Var))$, $i = \{1, 2\}$ and the coefficients of the battery cost-function are $a_P = a_Q = 1$. We assume that cost function (7) is the single grid-cost so that the assumptions of Theorem 3 are valid, with a target value $y^*_m = P_{DP} = -20$ kW. The forecast power to be generated by the PV is $\hat{\mathcal{P}}_{pv} = 30$ kW, the forecast consumption of the load is $\hat{\mathcal{P}}_{load} = -15$ kW, and their reactive power is assumed to be 0. The uncertainty in the slack power is assumed to be equal to the maximum value $\Delta y_m = |\Delta y_m|_{max} = 2$ kW.

Fig. 6 shows the value of $|y^{real}_m - y^*_m|$ obtained by solving the linearized optimization problem and the theoretical upper bound computed from Theorem 3 as a function of the weight w_m for different values of d taken from a logarithmic space between 1 W and 100 kW. Each continuous line represents one function $g(w_m, d)$, as defined in (24).

Now we assume that the desired upper bound for the tracking difference $|P_s - P_{DP}|$ is $d^*_{max,P_s} = 2.2$ kW (larger than $|\Delta y_m|_{max}$). According to Theorem 4, to compute the optimal weight, we need to consider only the function $g(w_m, d^*_{max} - |\Delta y_m|_{max})$, as shown separately in Fig. 6 (bottom graph). The optimal weight is the smallest one that gives $g(w_m, 200\ \text{W}) = 200\ \text{W} + |\Delta y_m|_{max}$, as computed by (32).

5.4. Multiple objectives

The method presented in Section 5.1 is only useful when the grid objective reflects a single grid variable. Practical applications, however, would typically involve multiple of such objectives. For the work studied in this paper, the computation of the total grid objective is based on certain heuristics. The individual objectives are the following: (i) slack-active-power cost, (ii) slack-reactive-power cost, (iii) average voltage cost of nodes, and (iv) average current cost of lines.

The first heuristic concerns costs (iii) and (iv). The idea is that adding a node or line to the grid should not affect, on average, the value of costs (iii) and (iv), respectively. Therefore, cost (iii) is computed as the weighted average of the costs $J_{V_k}, k = 1..K$ and cost (iv) is computed as the weighted average of the costs $J_{I_l}, l = 1..L$. The weights are computed individually for each objective by using formula (32).

The second heuristic is the following: if objectives (ii), (iii) and (iv) are equal to zero, then the upper bound computed from Theorem 3 should be true for objective (i). Similarly, if objective

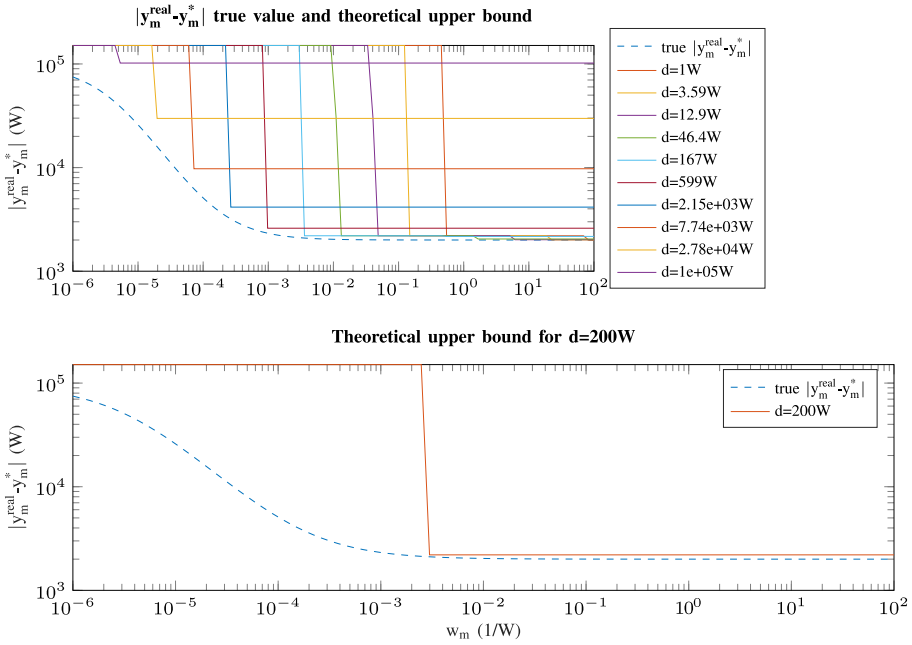

Fig. 6. True value of $|y_m^{real} - y_m^*|$ and theoretical upper bound as a function of the weight w_m, for different values of d. The curve corresponding to the desired upper bound is the one for $d = d^*_{max,m} - \Delta|y_m|_{max} = 200$ W and is shown in the bottom plot.

(i) is equal to zero, then the upper bound should hold for objective (ii). These two heuristics lead us to the total grid cost function:

$$\begin{aligned} J(\boldsymbol{x}|\boldsymbol{u}) =& w_{P_s} J_{P_s}(\boldsymbol{x}|\boldsymbol{u}) + w_{Q_s} J_{Q_s}(\boldsymbol{x}|\boldsymbol{u}) + \\ &+ \frac{1}{K}\sum_{k=1}^{K} w_{V_k} J_{V_k}(\boldsymbol{x}|\boldsymbol{u}) + \\ &+ \frac{1}{L}\sum_{l=1}^{L} w_{I_l^+} J_{I_l^+}(\boldsymbol{x}|\boldsymbol{u}) + w_{I_l^-} J_{I_l^-}(\boldsymbol{x}|\boldsymbol{u}) \end{aligned} \tag{33}$$

where the weights $w_{P_s}, w_{Q_s}, w_{V_k}, w_{I_l^+}, w_{I_l^-}$ are computed by formula (32) as if each objective was the single grid objective.

6. Numerical validation

6.1. Evaluation metrics

In order to compare our method with the "oracle" presented in Section 3, we define certain metrics that can be computed a posteriori for the interval $[\tau, \tau + \Delta T]$. For grid objectives, the metric is chosen so that the value is < 1 when $|y_m^{real}(t) - y_m^*(t)| > d^*_{max,m}(\tau)$.

$$metric\_grid_m = \frac{1}{\Delta T}\int_{t=\tau}^{\tau+\Delta T} \frac{|y_m^{real}(t) - y_m^*(t)|}{d^*_{max,m}(\tau)} dt \tag{34}$$

For batteries, the metric needs to evaluate two things, specifically (i) the satisfaction of each individual battery objective and (ii) the fairness between the two objectives. Assuming only two batteries, we can construct the metric given the vectors $\vec{r_P} = (|r_{P,1}|, |r_{P,2}|)$ and $\vec{r_Q} = (|r_{Q,1}|, |r_{Q,2}|)$ where $r_{P,i}, r_{Q,i}$ are the preference ratios of battery i defined in (13).

$$metric\_batt_P = \frac{1}{\Delta T}\int_{t=\tau}^{\tau+\Delta T} |\vec{r_P}(t)| \frac{cos(4\angle\vec{r_P}(t)) + 3}{8}\, dt \tag{35}$$

and similarly for the reactive power. These metrics are designed so that they take values in [0, 1] with increasing values indicating worse performance. In particular, the value 0 is taken only when $|\vec{r_P}(t)| = 0$ (similarly when $|\vec{r_Q}(t)| = 0$), while the value 1 is taken when either $|r_{P,1}| = 0$, $|r_{P,1}| = 2$ or $|r_{P,1}| = 2$, $|r_{P,1}| = 0$ (similarly for Q).

6.2. Evaluation of the proposed method in the scenario of Section 3

We consider the same microgrid as in Section 3; it is shown in Fig. 1. Using the same scenario for the uncontrollable resources and the slack voltage profile, we perform simulations over a 15-min period. This time, we use cost functions for the batteries in the form (15), and the total grid objective is computed as in Eq. (33).

We assume again that the batteries have received a target SoC from the intra-day layer, and we adapt the cost function (6) to satisfy the form (15). The preference of battery i is computed as follows:

$$P_i^*(\Delta SoC, \epsilon_i) = \begin{cases} -\frac{S_i}{\sqrt{2}} & \Delta SoC_i \le -\epsilon_i \\ \frac{\Delta SoC_i}{\epsilon_i}\frac{S_i}{\sqrt{2}} & -\epsilon_i < \Delta SoC_i < \epsilon_i \\ \frac{S_i}{\sqrt{2}} & \Delta SoC_i \ge \epsilon_i \end{cases} \tag{36}$$

The purpose of ϵ_i is to prevent the preference from oscillating between $\pm S_i$ when $\Delta SoC \simeq 0$. An appropriate condition for this purpose is $\epsilon_i > \frac{S_i T}{E_{max,i}}$, where $E_{max,i}$ is the energy capacity of the battery and $T = 10$ s is the time interval between two computation cycles.

The parameters of the battery cost functions are the following: $\epsilon_1 = \epsilon_2 = 1/360$, $a_P = a_Q = 1$. The parameters related to the various grid objectives, as defined in Section 5.2 are the following: $|P_s - P_{DP}|_{max} = 1.1|\Delta P_s|_{max}$, $|Q_s|_{max} = 1.1|\Delta Q_s|_{max}$, $\beta_{hard} = 0.05$ pu, $\beta_{soft} = 0.04$ pu and $\gamma_{soft} = 0.9$.

The simulation results are shown in Fig. 7. Concerning the plots of nodal voltages, branch currents, and nodal active and reactive power injections, there is no noticeable difference from those of Fig. 4. This means that our method achieves comparable results with the oracle-based approach, with the advantage of being grid and scenario-independent. Concerning the SoC plot, we observe a more fair regulation of the SoC of the two batteries, compared to Figs. 3 and 4. At the beginning of the simulation, the SoC is indeed the same for both batteries, due to the following factors: (i) Our design goal that the power setpoints should be proportional to the rated power of the battery, and (ii) the fact that the energy capacity of the batteries is proportional to their

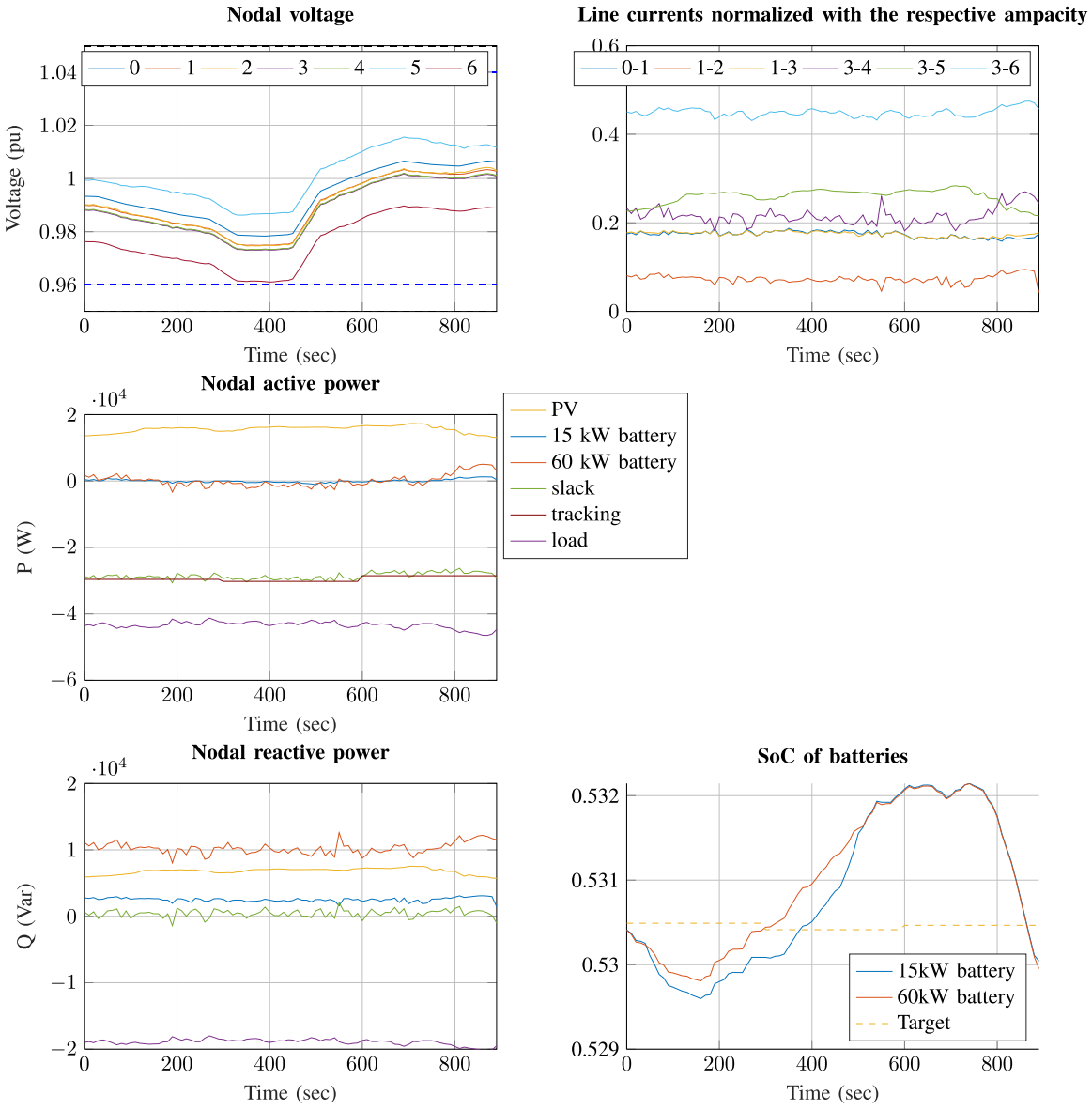

Fig. 7. Simulation results using our new cost functions.

Table 1
Values of metrics for the first scenario.

Method	Slack Q	Tracking	Voltage	Current	Battery P	Battery Q	Average
Same Weights	4.7579	6.4178	0.27263	0.17848	0.4023	0.042088	2.0119
Oracle-based	0.40798	0.51891	0.31589	0.19106	0.21783	0.10926	0.29349
Proposed method	0.43838	0.49225	0.31578	0.18932	0.11987	0.060715	0.26939

rated power. However, as time progresses, the small battery slows down its charging. This occurs because the controller instructs the smaller battery to compensate for the voltage drop, as bus 2 has an impact on the voltage objective higher than bus 4. This creates a temporary imbalance between the SoCs of the two batteries that is fixed after the voltage drop.

Here, we compute the metrics defined in Section 6.1 for the three cases, specifically (i) the cost functions of Section 3.1 with equal weights for all objectives, (ii) the oracle-based approach and (iii) the proposed cost functions. Their values are shown in Table 1. Our method achieves smaller values for all metrics, except the slack-reactive-power metric. This result verifies that our method can achieve comparable performance with the (less practical) oracle-based approach.

6.3. Evaluation of the proposed method in a different scenario

To further justify the merit of the proposed method, we apply it to another case study, specifically the work of Borghetti et al. [12]. This case is similar to the one studied in our work, as (i) it considers a multi-layer control approach and (ii) it considers both individual resources and both global grid objectives. Moreover, Borghetti et al. do not give any insight into how they chose the weights of the objectives.

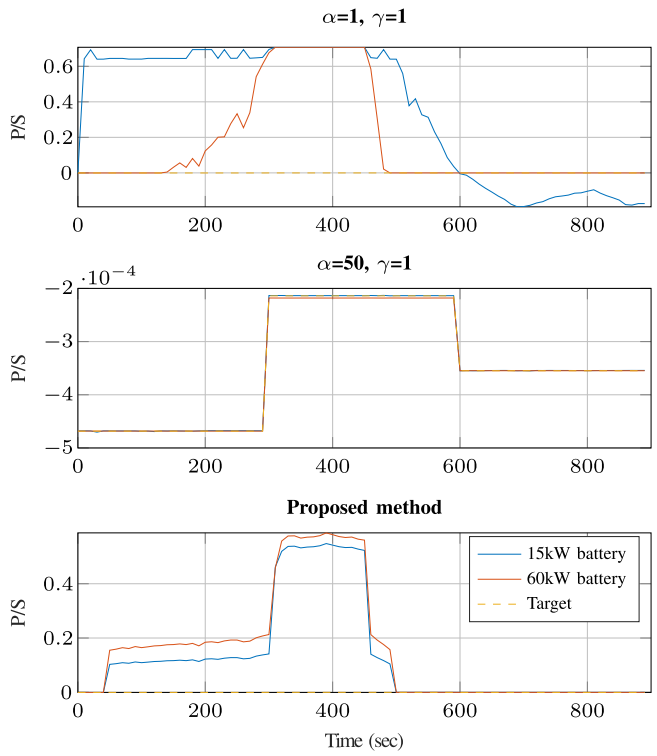

Fig. 8. Simulation results for the problem defined in [12] for three different weight configurations.

The control consists of two layers, namely (i) day-ahead and (ii) intra-day. The first layer computes a target power trajectory for each energy resource in the grid to be followed by the second layer. The second layer is also responsible for minimizing voltage deviations from the nominal value. Here, we target a simplification of the problem defined in [12]. We consider the grid of Fig. 1, where the target trajectory of each battery was computed by [18]. The target objective is

$$\min_{P_j} \sum_{j=1}^{N} \alpha |P_j - \bar{P}_j| + \sum_{i=1}^{N_{bus}} \gamma |V_i - 1| \tag{37}$$

where P_j and $\bar{P}_j$ are the computed and target power of battery j, respectively, and V_i is the voltage of bus i. We consider the same scenario for the load, PV, and slack voltage, as in Section 6.

Borghetti et al. consider two sets of values for the weights α and γ, namely (i) $\alpha = 1, \gamma = 1$ and (ii) $\alpha = 50, \gamma = 1$. Fig. 8 shows the evolution of the battery power trajectories and their respective targets normalized by the rated power of each battery for these two cases. When the two weights are equal, the controller forces the small battery to produce at its maximum power ($\frac{\sqrt{2}}{2}S$) to compensate for the voltage drop. Whereas, when $\alpha = 50$, the two trajectories match their target value, meaning that the controller fails at regulating the voltage.

To test our method, we first need to convert the absolute values of Eq. (37) to square functions, to satisfy our guidelines. The results with our method are also shown in Fig. 8. Concerning voltage regulation, our method achieves a control that, between the two batteries, is more fair than the manual-weight-tuning approach (the ratios P/S are very close).

7. Conclusion

We have defined guidelines for the design of objectives for the real-time control of batteries in a microgrid and have proposed a method for computing their weights. Our method requires only certain parameters as input that can be chosen intuitively and achieves a comparable performance to oracle-based approaches that are usually applied by the existing literature and are not feasible in practice. Because the method is grid-agnostic, we have also shown it can easily be applied to different problems, hence it can be employed by others in the future.

In future research, we plan to address the limitations of our method, concerning the types of objectives considered. Currently, the method is limited to batteries with the same objective, which is to regulate their SoC for the purpose of dispatchability. It would be interesting to study the case where batteries have different objectives, for example, the case where one battery acts as the slack bus. We also plan to extend the method to consider different types of energy resources, as well as long-term objectives, to guarantee the fair satisfaction of objectives in the long run.

CRediT authorship contribution statement

Plouton Grammatikos: Conceptualization, Methodology, Software, Validation, Investigation, Writing – original draft. **Mario Paolone:** Conceptualization, Writing – review & editing, Supervision. **Jean-Yves Le Boudec:** Conceptualization, Writing – review & editing, Supervision.

Declaration of competing interest

The authors declare that they have no known competing financial interests or personal relationships that could have appeared to influence the work reported in this paper.

Data availability

Data will be made available on request.

Acknowledgments

This research is carried out in the frame of the "Optimal integration of electric vehicles fast charging stations into medium voltage power distribution grids" project, with the financial support of the Swiss Federal Office of Energy (SFOE Pilot and Demonstration Program) (SI/502045-01) as a contribution to the ERA-NET project, "MESH4U - Multi Energy Storage Hub For reliable and commercial systems Utilization) (MICall19 - 100522)".

Appendix. Proofs of theorems

A.1. Proof of Theorem 1

Because the optimization problem is assumed to be unconstrained, the optimal solution would be a stationary point of the cost function. This means that for every battery i we should have:

$$\frac{\partial C_t(\boldsymbol{x}^{opt}|\hat{\boldsymbol{u}})}{\partial P_i} = \frac{\partial C_t(\boldsymbol{x}^{opt}|\hat{\boldsymbol{u}})}{\partial Q_i} = 0 \tag{38}$$

From the form of the total cost-function (2) and the battery cost-function (15), we have the following set of equations $\forall i = 1..N$:

$$\begin{aligned} \frac{\partial C_t(\boldsymbol{x}^{opt}|\hat{\boldsymbol{u}})}{\partial P_i} &= a_P \frac{r_{P,i}}{2} + \frac{\partial J(\boldsymbol{x}^{opt}|\hat{\boldsymbol{u}})}{\partial P_i} \\ \frac{\partial C_t(\boldsymbol{x}^{opt}|\hat{\boldsymbol{u}})}{\partial Q_i} &= a_Q \frac{r_{Q,i}}{2} + \frac{\partial J(\boldsymbol{x}^{opt}|\hat{\boldsymbol{u}})}{\partial Q_i} \end{aligned} \tag{39}$$

where $r_{P,i}$ is defined in (13). Given the sets of Eqs. (38) and (39), we get Eqs. (14) with $\lambda_P = -\frac{2}{a_P}$ and $\lambda_Q = -\frac{2}{a_Q}$, which is the statement of the theorem.

A.2. Proof of Theorem 2

We present the proof for inequality (18). Assuming cost function (15), we compute the derivative of the total cost function C_t with respect to P_m, $m \in \{i, j\}$.

$$\frac{\partial C_t}{\partial P_m} = a_P \frac{r_{P,m}}{2} + \frac{\partial J(\boldsymbol{x}|\boldsymbol{u})}{\partial P_m} \tag{40}$$

where $r_{P,m}$ is defined in (13). We consider all the possible cases that might hold at the optimum $\boldsymbol{x}^{opt}$:

(a)

$$\frac{\partial C_t(\boldsymbol{x}^{opt}|\hat{\boldsymbol{u}})}{\partial P_m} = 0, m \in \{i, j\}$$

By setting Eq. (40) equal to 0 for both batteries and considering condition (16), we verify that the upper bound of inequality (18) is achieved. This case is met under the assumption of Theorem 1.

(b)

$$\frac{\partial C_t(\boldsymbol{x}^{opt}|\hat{\boldsymbol{u}})}{\partial P_i} \cdot \frac{\partial C_t(\boldsymbol{x}^{opt}|\hat{\boldsymbol{u}})}{\partial P_j} > 0$$

If the derivative of the total cost function with respect to P_i at the optimum is strictly positive, this means that the value of P_i cannot be decreased further, which implies that it should take its minimum value, i.e.

$$\frac{P_i^{opt}}{S_i} = (\frac{P}{S})_{min}$$

On the other hand, if the derivative is negative, then

$$\frac{P_i^{opt}}{S_i} = (\frac{P}{S})_{max}$$

Since the derivatives of C_t with respect to P_i and P_j have the same sign, and considering assumptions (16) and (17), we get that in both of these cases we have $r_{P,i} = r_{P,j}$. Hence, inequality (18) is satisfied.

(c)

$$\frac{\partial C_t(\boldsymbol{x}^{opt}|\hat{\boldsymbol{u}})}{\partial P_i} > 0, \frac{\partial C_t(\boldsymbol{x}^{opt}|\hat{\boldsymbol{u}})}{\partial P_j} = 0$$

Using the explanation of the previous point, we should have only for battery i

$$\frac{P_i^{opt}}{S_i} = (\frac{P}{S})_{min}$$

and given assumption (17) we should have:

$$r_{P,i} - r_{P,j} \leq 0 \tag{41}$$

Moreover we should have:

$$\begin{aligned} &\frac{\partial C_t(\boldsymbol{x}^{opt}|\hat{\boldsymbol{u}})}{\partial P_i} - \frac{\partial C_t(\boldsymbol{x}^{opt}|\hat{\boldsymbol{u}})}{\partial P_j} > 0 \implies \\ &\frac{a_P}{2}(r_{P,i} - r_{P,j}) > -(\frac{\partial J(\boldsymbol{x}^{opt}|\hat{\boldsymbol{u}})}{\partial P_i} - \frac{\partial J(\boldsymbol{x}^{opt})}{\partial P_j}) \end{aligned} \tag{42}$$

Combining (41) and (42), we derive that both sides of inequality (42) are negative, therefore, taking the absolute value results in the desired condition (18).

(d)

$$\frac{\partial C_t(\boldsymbol{x}^{opt}|\hat{\boldsymbol{u}})}{\partial P_i} < 0, \frac{\partial C_t(\boldsymbol{x}^{opt})}{\partial P_j} = 0$$

We can work in a similar way as case (d) and show that

$$r_{P,i} - r_{P,j} \geq 0 \tag{43}$$

and

$$\frac{a_P}{2}(r_{P,i} - r_{P,j}) < -(\frac{\partial J(\boldsymbol{x}^{opt}|\hat{\boldsymbol{u}})}{\partial P_i} - \frac{\partial J(\boldsymbol{x}^{opt}|\hat{\boldsymbol{u}})}{\partial P_j}) \tag{44}$$

Now, both scales of inequality (44) are positive so taking the absolute value results once again in condition (18).

(e)

$$\frac{\partial C_t(\boldsymbol{x}^{opt}|\hat{\boldsymbol{u}})}{\partial P_i} \cdot \frac{\partial C_t(\boldsymbol{x}^{opt}|\hat{\boldsymbol{u}})}{\partial P_j} < 0$$

The proof follows in the same way as in cases (c)–(d). In particular, we can show that either (41) and (42) will hold together or (43) together with (44).

We have, thus, concluded that inequality (18) should hold for every possible values of $\frac{\partial C_t(\boldsymbol{x}^{opt}|\hat{\boldsymbol{u}})}{\partial P_m}$, $m \in \{i, j\}$. The same method can be used to prove the result for the reactive power.

A.3. Proof of Lemma 1

We assume that for some value $d > 0$ we have

$$|y_m^{opt} - y_m^*| > d \tag{45}$$

which can be rewritten as:

$$\begin{aligned} &y_m^{opt} > y_m^* + d \\ \text{or } &y_m^{opt} < y_m^* - d \end{aligned} \tag{46}$$

Because J_m is a convex function by design, then its derivative J_m' is an increasing function, which means that:

$$\begin{aligned} &J_m'(y_m^{opt}) > J_m'(y_m^* + d) \\ \text{and } &J_m'(y_m^{opt}) < J_m'(y_m^* - d) \end{aligned} \tag{47}$$

Moreover, because $J_m(y_m + y_m^*)$ is also an even function by design, then $J_m'(y_m + y_m^*)$ is an odd function. This means that

$$J_m'(y_m^* + d) = -J_m'(y_m^* - d), \forall d \tag{48}$$

Combining conditions (47) and (48), we get

$$|J_m'(y_m^{opt})| > |J_m'(y_m^* \pm d)|, \forall d \tag{49}$$

We consider any variable $x_j \in \{P_j, Q_j\}$, i.e. it represents either the active or the reactive power of battery j, such that the respective sensitivity coefficient satisfies the inequality $|K_{x,j}^m| \geq K_t(d, w_m)$. Then, we compute the following quantity

$$w_m |\frac{\partial J(\boldsymbol{x}^{opt}|\hat{\boldsymbol{u}})}{\partial x_j}| \overset{(22)}{=} \frac{|J_m'(y_m^{opt})|}{|J_m'(y_m^* + d)|} \frac{|K_{x,j}^m|}{K_t(d, w_m)} \overset{(49)}{>} 1 \tag{50}$$

Considering the battery cost-function (15) with $a_{P,j}, a_{Q,j} \in (0, 1], \forall j$ and the fact that for every battery we have $P_j, Q_j \in [-S_j, S_j]$ we derive the following inequality

$$w_j |\frac{\partial C_j}{\partial x_j}| \leq 1, \forall j \tag{51}$$

From inequalities (50) and (51) we infer that we should have one the following two cases:

$$w_m \frac{\partial J(\boldsymbol{x}^{opt}|\hat{\boldsymbol{u}})}{\partial x_j} > 1 \implies x_j^{opt} = x_{j,min} \tag{52}$$

$$w_m \frac{\partial J(\boldsymbol{x}^{opt}|\hat{\boldsymbol{u}})}{\partial x_j} < -1 \implies x_j^{opt} = x_{j,max} \tag{53}$$

This result follows from the box form of the constraints of the problem in the same way as in case (b) of the proof of Theorem 2.

Now, we consider the following two cases:

(A) $J'_m(y_m^{opt}) > 0$
In this case, for any variable x_j, with $|K_{x,j}^m| \geq K_t$ we have

$$\begin{cases} K_{x,j}^m > 0 \xrightarrow{(52)} x_j^{opt} = x_{j,min} \\ K_{x,j}^m < 0 \xrightarrow{(53)} x_j^{opt} = x_{j,max} \end{cases}$$

Therefore, no matter what is the value of the sensitivity $K_{x,j}^m$, the product $K_{x,j}^m x_j^{opt}$ takes the minimum possible value, which we denote as $K_{x,j}^m x_j^{opt} = (K_{x,j}^m x_j)_{min}$.
The next step is to examine the ordering of the following three points, namely (i) the value of y_m evaluated at the optimal solution y_m^{opt}, (ii) its minimum value within the domain of the problem y_m^{min} and (iii) the value that minimizes the grid cost within the same domain y_m^{inf}. Now we consider two cases regarding the point y_m^{inf}:

i. The point that minimizes J_m is not stationary, i.e. $J'_m(y_m^{inf}) \neq 0$. Then, variable y_m must be constrained. Because $J'_m(y_m^{opt}) > 0$ by assumption, y_m must be constrained by its lower bound y_m^{min}, i.e. $y_m^{inf} = y_m^{min}$ and since y_m^{opt} is within the domain of y_m, we derive the ordering of the points as $y_m^{min} = y_m^{inf} \leq y_m^{opt}$
ii. The point is stationary, i.e. $J'_m(y_m^{inf}) = 0$. Then variable y_m is not constrained, which means that $y_m^{inf} \geq y_m^{min}$ and $y_m^{opt} \geq y_m^{min}$. Now, considering the assumption that $J'_m(y_m^{opt}) > 0 = J'_m(y_m^{inf})$ and the fact that J'_m is an increasing function (by convexity), we get the following ordering of the points $y_m^{min} \leq y_m^{inf} < y_m^{opt}$

The ordering derived above can be re-written in the following way

$$J'_m(y_m^{opt}) > 0 \implies |y_m^{opt} - y_m^{inf}| \leq |y_m^{opt} - y_m^{min}| \tag{54}$$

We can continue to show that

$$\begin{aligned} &|y_m^{opt} - y_m^*| \leq |y_m^* - y_m^{inf}| + |y_m^{opt} - y_m^{inf}| \leq \\ &\leq |y_m^* - y_m^{inf}| + \\ &+ |\sum_i K_{x,i}^m x_i^{opt} - \sum_i (K_{x,i}^m x_i)_{min}| \leq \\ &\leq |y_m^* - y_m^{inf}| + \\ &+ \sum_{|K_{x,i}^m| < K_t(d,w_m)} |K_{x,i}^m||x_{i,max} - x_{i,min}| \end{aligned} \tag{55}$$

(B) $J'_m(y_m^{opt}) < 0$
We can show in a similar way, that in this case, we have $K_{x,j}^m x_j^{opt} = (K_{x,j}^m x_j)_{max}$ for any variable x_j with $|K_{x,j}^m| \geq K_t$ and that:

$$J'_m(y_m^{opt}) < 0 \implies |y_m^{opt} - y_m^{inf}| \leq |y_m^{opt} - y_m^{max}| \tag{56}$$

From this, we can show that we get again inequality (55). Since the above inequalities are true for any $d > 0$, we can take as upper bound the minimum of these bounds over all values d. Hence, we get the upper bound $f(w_m)$.

A.4. Proof of Theorem 3

By taking definition (27) and applying the triangle inequality we get

$$\begin{aligned} |y_m^{real} - y_m^*| &= |y_m^{opt} - \Delta y_m - y_m^*| \leq \\ &\leq |y_m^{opt} - y_m^*| + |\Delta y_m| \leq \\ &\leq |y_m^{opt} - y_m^*| + |\Delta y_m|_{max} \end{aligned} \tag{57}$$

and from Lemma 1, we have

$$|y_m^{opt} - y_m^*| \leq f(w_m) \tag{58}$$

Combining the above two conditions, we get the statement of the theorem.

A.5. Proof of Theorem 4

Let w_m^* be a solution to Problem 2. Considering the nature of the problem, this solution is the minimum value of w_m that satisfies a constraint, therefore it should be unique. By definition (29) we have

$$f_u(w_m^*) = \min_d g(w_m^*, d) + |\Delta y_m|_{max} \tag{59}$$

Now, by evaluating $g(w_m^*, d)$ at $d = d_{max}^* - |\Delta y_m|_{max}$ we get

$$f_u(w_m^*) \leq g(w_m^*, d_{max,m}^* - |\Delta y_m|_{max}) + |\Delta y_m|_{max} \tag{60}$$

Also, because w_m^* is a solution to Problem 2, it should satisfy constraint (31). Combining it with the previous inequality we have

$$f_u(w_m^*) \leq d_{max,m}^* - |\Delta y_m|_{max} + |\Delta y_m|_{max} = d_{max,m}^* \tag{61}$$

which is equivalent to (30). Therefore, w_m^* also satisfies the constraint of Problem 1.

Now, we assume another weight $w'_m \in (0, w_m^*)$ and denote $\Delta d_{max,m}^* = d_{max,m}^* - |\Delta y_m|_{max}$, for ease of notation. We will show that w'_m cannot satisfy the constraint of Problem 1. Let $d > 0$ be an arbitrary value. We consider the following two cases

(1) $d > \Delta d_{max,m}^*$
By the definition of function g in (24) we have

$$g(w'_m, d) = \max\{d, h(K_t(w'_m, d))\} \geq d > \Delta d_{max,m}^* \tag{62}$$

(2) $d < \Delta d_{max,m}^*$
By the definition of function K_t in (22) and the fact that J'_m is an increasing function (by convexity of J_m) we see that for a given argument w_m the function $K_t(w_m, d)$ is strictly decreasing for $d > 0$. And because we consider the case where $d < \Delta d_{max,m}^*$ we should have

$$K_t(w'_m, d) > K_t(w'_m, \Delta d_{max,m}^*) \tag{63}$$

Now, from the definition of h in (23) we can derive that $h(K)$ is increasing in K, so from (63) we get

$$h(K_t(w'_m, d)) \geq h(K_t(w'_m, \Delta d_{max,m}^*)) \tag{64}$$

Because $w'_m < w_m^*$ and w_m^* is the solution to Problem 2, then w'_m should not satisfy constraint (31). Therefore, by using the term $\Delta d_{max,m}^*$ we defined in this proof we get

$$g(w'_m, \Delta d_{max,m}^*) > \Delta d_{max,m}^* \tag{65}$$

Also, from the definition of g, we have

$$\begin{aligned} &g(w'_m, \Delta d_{max,m}^*) = \\ &\max\{\Delta d_{max,m}^*, h(K_t(w'_m, \Delta d_{max,m}^*))\} \end{aligned} \tag{66}$$

and taking into account the last two conditions, we can infer that

$$h(K_t(w'_m, \Delta d_{max,m}^*)) > \Delta d_{max,m}^* \tag{67}$$

Combining all the above results, we get

$$\begin{aligned} &g(w'_m, d) = \max\{d, h(K_t(w'_m, d))\} \geq \\ &\geq h(K_t(w'_m, d)) \geq h(K_t(w'_m, \Delta d_{max,m}^*)) \geq \\ &\geq \Delta d_{max,m}^* > d \end{aligned} \tag{68}$$

Hence, we get $g(w'_m, d) > \Delta d_{max,m}^* \forall d \neq \Delta d_{max,m}^*$ and given the definition of $f_u(w_m)$ in (29) we have

$$f_u(w'_m) > d_{max,m}^*, \forall w'_m < w_m^* \tag{69}$$

which means that any $w'_m < w_m^*$ cannot be the solution to Problem 1. Therefore, w_m^* is also the solution to Problem 1.

References

[1] F. Pilo, S. Jupe, F. Silvestro, et al., Planning and Optimization Methods for Active Distribution Systems, Paris, France, 2014, WG C6.19: Tb 591, Cigre.

[2] K. Tazi, F. Abbou, F. Abdi, Multi-agent system for microgrids: design, optimization and performance, 2020,

[3] T.L. Vandoorn, B. Meersman, J.D.M.D. Kooning, L. Vandevelde, Directly-coupled synchronous generators with converter behavior in islanded microgrids, IEEE Trans. Power Syst. 27 (2012) 1395–1406.

[4] T. Logenthiran, D. Srinivasan, A. Khambadkone, H. Aung, Multiagent system for real-time operation of a microgrid in real-time digital simulator, 2012.

[5] G. Valverde, T. Van Cutsem, Model predictive control of voltages in active distribution networks, IEEE Trans. Smart Grid 4 (2013) 2152–2161.

[6] M. Bozorg, F. Sossan, J.-Y. Le Boudec, M. Paolone, Influencing the bulk power system reserve by dispatching power distribution networks using local energy storage, Electr. Power Syst. Res. 163 (2018) 270–279, URL https://www.sciencedirect.com/science/article/pii/S0378779618301901.

[7] E. Stai, F. Sossan, E. Namor, J.-Y.L. Boudec, M. Paolone, A receding horizon control approach for re-dispatching stochastic heterogeneous resources accounting for grid and battery losses, Electr. Power Syst. Res. 185 (2020) 106340, URL https://www.sciencedirect.com/science/article/pii/S0378779620301462.

[8] M. Cintuglu, T. Youssef, O. Mohammed, Development and application of a real-time testbed for multiagent system interoperability: A case study on hierarchical microgrid control, in: 2017 IEEE Power Energy Society General Meeting, 2017, p. 1.

[9] B. Zhao, X. Zhang, J. Chen, C. Wang, L. Guo, Operation optimization of standalone microgrids considering lifetime characteristics of battery energy storage system, IEEE Trans. Sustain. Energy 4 (4) (2013) 934–943.

[10] R. de Azevedo, M.H. Cintuglu, T. Ma, O.A. Mohammed, Multiagent-based optimal microgrid control using fully distributed diffusion strategy, IEEE Trans. Smart Grid 8 (4) (2017) 1997–2008.

[11] C.M. Colson, M.H. Nehrir, Comprehensive real-time microgrid power management and control with distributed agents, IEEE Trans. Smart Grid 4 (1) (2013) 617–627.

[12] A. Borghetti, M. Bosetti, S. Grillo, S. Massucco, C.A. Nucci, M. Paolone, F. Silvestro, Short-term scheduling and control of active distribution systems with high penetration of renewable resources, IEEE Syst. J. 4 (3) (2010) 313–322.

[13] K. Zhang, W. Shi, H. Zhu, E. Dall'Anese, T. Başar, Dynamic power distribution system management with a locally connected communication network, IEEE J. Sel. Top. Sign. Proces. 12 (4) (2018) 673–687.

[14] A. Bernstein, L. Reyes-Chamorro, J.-Y. Le Boudec, M. Paolone, A composable method for real-time control of active distribution networks with explicit power setpoints. Part I: Framework, Electr. Power Syst. Res. 125 (2015) 254–264.

[15] R. Rudnik, J. Le Boudec, A. Bernstein, L. Reyes-Chamorro, M. Paolone, Handling large power steps in real-time microgrid control via explicit power setpoints, in: 2017 IEEE Manchester PowerTech, 2017, pp. 1–6.

[16] K. Christakou, J.-Y. LeBoudec, M. Paolone, D.-C. Tomozei, Efficient computation of sensitivity coefficients of node voltages and line currents in unbalanced radial electrical distribution networks, IEEE Trans. Smart Grid 4 (2) (2013) 741–750.

[17] https://github.com/DESL-EPFL/Testbed-microgrid-for-cost-functions-evaluation.

[18] E. Stai, L. Reyes-Chamorro, F. Sossan, J.-Y. Le Boudec, M. Paolone, Dispatching stochastic heterogeneous resources accounting for grid and battery losses, IEEE Trans. Smart Grid 9 (6) (2018) 6522–6539.

[19] L.E. Reyes Chamorro, Real-Time Control Framework for Active Distribution Networks Theoretical Definition and Experimental Validation, EPFL, Lausanne, 2016, p. 176, URL http://infoscience.epfl.ch/record/221619.

[20] A. Nurkanovic, A. Mešanovic, A. Zanelli, G. Frison, J. Frey, S. Albrecht, M. Diehl, Real-time nonlinear model predictive control for microgrid operation, 2020.